공학석사 학위논문

Catalytic activation of peroxymonosulfate by hematite for oxidation of organic compounds

오염물질의 분해를 위한 헤마타이트의 일과황산염 활성화

2021년 2월

서울대학교 대학원

공과대학 화학생물공학부 화학생물공학 전공

강 현 석

Catalytic activation of peroxymonosulfate by hematite for oxidation of organic compounds

오염물질의 분해를 위한 헤마타이트의 일과황산염 활성화

지도교수 이 창 하

이 논문을 공학석사 학위논문으로 제출함

2020 년 12 월

서울대학교 대학원
공과대학 화학생물공학부 화학생물공학 전공
강 현 석

강현석의 석사 학위논문을 인준함

2021 년 1 월

위 원 장 오 준 학 (인)

부위원장 이 창 하 (인)

위 원 이 규 태 (인)

ABSTRACT

Catalytic activation of peroxymonosulfate by hematite for oxidation of organic compounds

Kang Hyeonseok

School of Chemical and Biological Engineering

The Graduate School

Seoul National University

Hematite (α-Fe_2O_3) was found to activate peroxymonosulfate (PMS) for oxidizing organic compounds in aqueous environments. α-Fe_2O_3 activated PMS can effectively degrade phenolic compounds (i.e., phenol, bisphenol A, and 2,4,6-trichlorophenol). The effects of pH, catalyst dosage, and PMS concentration on phenol degradation were investigated. The observations obtained in this study provided evidence against the generation of reactive species such as sulfate radical, hydroxyl radical, superoxide radical, and singlet oxygen. Radical scavenger (i.e., *tert*-butanol, methanol, and *p*-benzoquinone) test, superoxide radical probe test, anion (i.e., $H_2PO_4^-$,

ClO_4^-, NO_3^- and Cl^-) test, and electron paramagnetic resonance spectroscopy suggest that the oxidation mechanism does not likely involve the previously proposed radical mechanisms. Although singlet oxygen scavengers (i.e., furfuryl alcohol, azide ion, and L-histidine) could inhibit the phenol degradation, EPR spectroscopy and deuterium oxide test deny the responsible for singlet oxygen in α-Fe_2O_3/PMS system. PMS decomposition by α-Fe_2O_3 and electrochemical analysis rebuff the electron mediated reactive complex. Based on the observations from this study, it is suggested that a high-valent iron species (Fe(IV)) is the reactive species of the α-Fe_2O_3/PMS system. Fe^{IV}=O generated on the surface of α-Fe_2O_3 appears to be the responsible oxidant for the degradation of organic contaminants.

Keywords : Peroxymonosulfate, Hematite, Oxidation, Organic compounds, Nonradical mechanism, High-valent iron

***Student Number* : 2019-2765**

CONTENTS

List of figures

List of tables

1. Introduction

Advanced oxidation processes (AOPs) utilizing peroxymonosulfate (PMS) as an alternative oxidant for organic contaminants degradation have attracted attention due to high reactivity and stability [1–4]. PMS has a high redox potential ($E°(HSO_5^-/SO_4^{2-})$ = 1.75 V *vs.* NHE [5]) that has the ability to direct oxidation of organic pollutants [5–9]. PMS can further be activated to generate $SO_4^{\bullet-}$ ($E°(SO_4^{\bullet-}/SO_4^{2-})$ = 2.43 V *vs.* NHE [6]) that is more effective, fast, but nonselective, through various activation methods (i.e., heat [10], base [11], UV [12], ultrasound [13], and transition metal [2–4]).

Iron has widely studied because of its low price, nontoxicity, and efficiency [14,15]. Iron-mediated persulfate activation can be applied in the remediation of pollutants in water and soil [3,16–18]. However, using iron ions has some limitations such as excessive iron ions rather reduce reactivity or the precipitated iron ions decrease the efficiency. Accordingly, heterogeneous iron oxide which works well in near-neutral pH is an alternative [19–21]. In particular, iron oxide is one of the abundant minerals consisting of the Earth's crust, so oxidant activation by iron oxide is a promising method for *in-situ* chemical oxidation (ISCO) [22].

Previously, PMS activation by iron(III) oxide (Fe_2O_3) and additives were studied by many researchers. The reactive species and the corresponding evidence that supporting the reaction mechanisms were proposed (Table 1).

Table 1

Previous studies on the PMS activation by iron(III) oxide.

Catalyst	Source of catalyst	Reactive species	Evidence for mechanism	Reference
Hematite	Commercially purchased	$SO_4^{\bullet-}$, $^{\bullet}OH$	Probe compound (Nitrobenzene) Scavenger (*tert*-butanol, Isopropanol)	[23]
Martite (α-Fe_2O_3)	Synthesized	$SO_4^{\bullet-}$	XPS (surface Fe(II) and Fe(III))	[15]
Porous Fe_2O_3	Synthesized	$SO_4^{\bullet-}$, $^{\bullet}OH$	Scavenger (*tert*-butanol, Methanol)	[14]
Nano Fe_2O_3	Synthesized	$SO_4^{\bullet-}$	Scavenger (*tert*-butanol, Ethanol) Anion (Cl^-, NO_3^-, HPO_4^{2-})	[24]
Dipicolinic acid-functionalized hematite	Synthesized	$SO_4^{\bullet-}$, $^{\bullet}OH$	-	[25]
γ-Fe_2O_3-montmorillonite	Synthesized	$SO_4^{\bullet-}$	-	[26]
Porous sulfurized Fe_2O_3	Synthesized	$SO_4^{\bullet-}$, $^{\bullet}OH$	Scavenger (*tert*-butanol, Methanol) EPR (DMPO) Anion (NO_3^-, Cl^-, HCO_3^-)	[27]
α-Fe_2O_3 + Cu_2O	Commercially purchased	$SO_4^{\bullet-}$, $^{\bullet}OH$	Scavenger (*tert*-butanol, Ethanol)	[28]
α-Fe_2O_3 + hydroxylamine	Commercially purchased	$SO_4^{\bullet-}$, $^{\bullet}OH$, $^1O_2$	Scavenger (*tert*-butanol, Methanol) EPR (DMPO, TEMP)	[29]
Ca-doped α-Fe_2O_3	Synthesized	$SO_4^{\bullet-}$, $^{\bullet}OH$, $O_2^{\bullet-}$, $^1O_2$	Scavenger (Methanol, *p*-benzoquinone, NaN_3) EPR (DMPO, TEMP, oxygen vacancy) Anion (HCO_3^-, $H_2PO_4^-$, NO_3^-, Cl^-)	[30]

For the pure form of Fe_2O_3, radical species were proposed as the main reactive species regardless of commercially purchased or synthesized [14,15,23,24]. Soltani et al. (2018) suggested that iron ions on the surface of martite nanoparticle proceed in the same mechanism as iron ions in an aqueous solution (Eqs. (1)–(3)) [15]. Ji et al. (2013) and Jaafarzadeh et al. (2017) explained the pathway of $SO_4^{\bullet-}$ generation from the reaction with surface iron and PMS (Eqs. (4)–(9)) [14,24]. On the other hand, recently, Sang et al. (2020) and Guo et al. (2020) suggested the contribution of a nonradical mechanism through singlet oxygen ($^1O_2$) in the system with Fe_2O_3 and additives [29,30]. In the meantime, a few studies suggested a radical mechanism only by the fact that it had known as a radical mechanism without any evidence. That is why more detailed studies on the activation mechanism are required.

$$Fe^{3+} + HSO_5^- \rightarrow SO_5^{\bullet-} + Fe^{2+} + H^+ \quad (1)$$

$$Fe^{2+} + HSO_5^- \rightarrow SO_4^{\bullet-} + Fe^{3+} + OH^- \quad (2)$$

$$SO_4^{\bullet-} + OH^- \rightarrow {}^{\bullet}OH + SO_4^{2-} \quad (3)$$

$$\equiv Fe^{III} + HSO_5^- \rightarrow SO_5^{\bullet-} + \equiv Fe^{II} + H^+ \quad (4)$$

$$\equiv Fe^{II} + HSO_5^- \rightarrow SO_4^{\bullet-} + \equiv Fe^{III} + OH^- \quad (5)$$

$$\equiv Fe^{III}\text{–}OH + HSO_5^- \rightarrow \equiv Fe^{III}\text{–}SO_5^- + H_2O \quad (6)$$

$$\equiv Fe^{III}\text{–}SO_5^- + H_2O \rightarrow SO_5^{\bullet-} + \equiv Fe^{II}\text{–}OH + H^+ \quad (7)$$

$$\equiv Fe^{II}\text{–}OH + HSO_5^- \rightarrow \equiv Fe^{II}\text{–}SO_5^- + H_2O \quad (8)$$

$$\equiv Fe^{II}\text{–}SO_5^- + H_2O \rightarrow SO_4^{\bullet-} + \equiv Fe^{III}\text{–}OH + OH^- \quad (9)$$

In this study, the catalytic activity of a-Fe_2O_3 as a PMS activator was investigated for the degradation of various organic compounds. The influence of water chemistry parameters was also tested. Various experiments including scavenger test, probe test, solvent test, anion test, electron paramagnetic resonance (EPR) spectroscopy, electrochemical analysis, and X-ray absorption near edge structure (XANES) spectroscopy were conducted to elucidate the pathway of PMS activation. Herein, we suggest the activation pathway does not involve radicals but occurs via a nonradical mechanism that is distinguished from previous studies.

2. Materials and methods

2.1. Reagents

All chemicals were reagent grade and used without further purification. Chemicals used in this study included: methanol (Honeywell) and oil-based carbon paste (BASi). PMS (Oxone, $KHSO_5 \cdot 0.5KHSO_4 \cdot 0.5K_2SO_4$), iron(III) oxide ($\alpha$-$Fe_2O_3$, hematite), iron(III) oxide-hydroxide (α-FeOOH, goethite), iron(II,III) oxide (Fe_3O_4, magnetite), iron(II) sulfate heptahydrate, iron(III) perchlorate hydrate, phenol, bisphenol A, benzoic acid, furfuryl alcohol, 2,4,6-trichlorophenol, 2,5-dimethylfuran, perchloric acid, sodium hydroxide, *tert*-butanol, *p*-benzoquinone, sodium azide (N_3^-), L-histidine, 2,3-bis(2-methoxy-4-nitro-5-sulfophenyl)-2*H*-tetrazolium-5-carboxanilide (XTT) sodium salt, deuterium oxide (D_2O), sodium phosphate monobasic, sodium perchlorate, sodium nitrate, sodium chloride, 5,5-dimethyl-1-pyrroline *N*-oxide (DMPO), 2,2,6,6-tetramethyl-4-piperidone hydrochloride (TEMPD•HCl), hydroxylamine solution were purchased from Sigma-Aldrich. Deionized (DI) water (18.2 MΩ cm, Millipore) was used to prepare all solutions.

2.2. EPR spectroscopy

EPR analysis was conducted using an EPR spectrometer (JES-X310, JEOL). 10 mM of spin trapping agent (i.e., DMPO and TEMPD•HCl) containing solution was prepared at aimed pH condition. PMS (1 mM) and α-Fe_2O_3 (5 g/L) were added to the solution to initiate the reaction. At predetermined time intervals, the samples were withdrawn and analyzed under the following conditions: microwave frequency = 9419 MHz; microwave power = 0.998 mW; modulation frequency = 100 MHz; and modulation amplitude = 2.0 G.

2.3. Electrochemical analysis

Linear sweep voltammetry (LSV) and cyclic voltammetry (CV) were performed using a potentiostat (VSP, Biologic). For the LSV test, a working electrode (glassy carbon electrode, GCE), a counter electrode (Pt foil), and a reference electrode (saturated calomel electrode, SCE) were used. While, a working electrode (carbon paste electrode, CPE), a counter electrode (Pt mesh), and a reference electrode (SCE) were used in the CV experiment. Perchlorate (50, 500 mM) was served as an electrolyte. Although SCE served as a reference electrode, the units and notations in this study were converted to a normal hydrogen electrode (NHE).

2.4. PMS treatment of α-Fe_2O_3 and characterization

PMS treatment of α-Fe_2O_3 was conducted to identify whether the reactive complex exists on the surface. α-Fe_2O_3 was immersed in a high concentration of PMS (200 mM) for more than 3 days. Then washed with DI water until no more PMS be detected and dried in the N_2 box overnight. The morphology and chemical property of pristine and PMS-treated α-Fe_2O_3 were characterized through high resolution transmission electron microscope-energy dispersive X-ray spectroscopy (HR-TEM/EDS, JEM-3010, JEOL), X-ray powder diffraction (XRD, D8 Discover, Bruker), surface zeta potential (Zetasizer Nano-ZS, Malvern), and XANES (R-XAS, Rigaku).

2.5. Experimental setup and procedure

All experiments were carried out in a 100 mL flask at room temperature (22 ± 1 °C). The reaction was initiated by adding 5 g/L α-Fe_2O_3 into the solution containing PMS (1 mM) and target contaminants (0.1 mM phenol, bisphenol A, benzoic acid, furfuryl alcohol, 2,4,6-trichlorophenol, 2,5-dimethylfuran) and conducted for 2 hours. In the presence of 1 mM PMS, the pH of the solution was about pH 3.3 and rarely changed during the reaction. The solution pH was adjusted with either $HOCl_4$ (0.1 M) or NaOH (0.1 M) if needed. During the process, 2mL of samples were collected at a predetermined time and filtered using 0.2 μm PTFE syringe filter to get rid of α-Fe_2O_3. The filtered samples were analyzed for PMS and target organic compounds.

2.6. Analytical methods

The concentration of target organic compounds was analyzed with ultrahigh performance liquid chromatography (UHPLC) with a UV-Vis detector (UltiMate 3000, Thermo Scientific). Acclaim 120 C18 rapid separation liquid chromatography column was used for separation. PMS and XTT were measured by UV-Vis spectrometer (Lambda 465, PerkinElmer). A modified colorimetric method was used for the detection of PMS [31].

3. Results and discussion

3.1. Degradation of organic compounds by α-Fe_2O_3/PMS system

The degradation of phenol by α-Fe_2O_3 in the presence of α-Fe_2O_3 and PMS was investigated at pH 3.3 (Fig. 1a). α-Fe_2O_3 or PMS alone system did not degrade phenol, indicating that the phenol removal by adsorption on the surface of α-Fe_2O_3 is negligible. Whereas, when both α-Fe_2O_3 and PMS existed, complete phenol degradation was achieved within 60 min. Furthermore, the efficiency of other iron-based catalysts such as ferrous ion (Fe(II)), ferric ion (Fe(III)), magnetite (Fe_3O_4), and goethite (α-FeOOH) was conducted in the presence of PMS (Fig. 1b). α-Fe_2O_3 was the most efficient catalyst, followed by α-FeOOH with 70% of phenol removal in 120 min, while other catalysts did not show effective phenol degradation.

Various organic compounds degradation by α-Fe_2O_3/PMS system was examined (Fig. 2a). Phenolic compounds (i.e., phenol, bisphenol A, 2,4,6-trichlorophenol, and 2,5-dimethylfuran) were effectively degraded by the system. However, benzoic acid and furfuryl alcohol were not completely degraded within 120 min (23% and 84% respectively). Pseudo-first-order rate constants (k) of organic compounds degradation observed by α-Fe_2O_3/PMS system are presented (Fig. 2b). Benzoic acid which has a high reactivity toward $SO_4^{\bullet-}$ and $^{\bullet}OH$ ($k_{SO_4^{\bullet-}}$ = 1.2 × 10^9 $M^{-1}s^{-1}$ and $k_{^{\bullet}OH}$ = 4.3 × 10^9 $M^{-1}s^{-1}$ [32,33]) and furfuryl alcohol which has a high reactivity toward $^1O_2$ ($k_{^1O_2}$ = 1.2 × 10^8 $M^{-1}s^{-1}$ [34]) were hardly degraded (Table 2). The selectivity toward these organic compounds indicates that $SO_4^{\bullet-}$, $^{\bullet}OH$, and $^1O_2$ are not involved

in the activation of PMS.

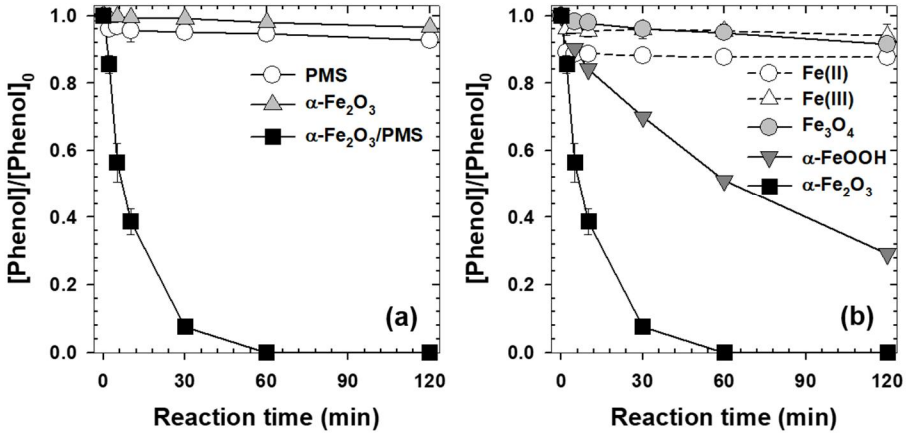

Fig. 1. (a) Degradation of phenol in the presence of α-Fe_2O_3 or/and PMS: $[Phenol]_0$ = 0.1 mM; $[\alpha\text{-}Fe_2O_3]_0$ = 5 g/L; $[PMS]_0$ = 1 mM; pH = 3.3. (b) Degradation of phenol by PMS in the presence of various iron-based catalysts: $[Phenol]_0$ = 0.1 mM; $[\alpha\text{-}Fe_2O_3]_0 = [Fe_3O_4]_0 = [\alpha\text{-}FeOOH]_0$ = 5 g/L; $[Fe(II)]_0 = [Fe(III)]_0$ = 0.1 mM; $[PMS]_0$ = 1 mM; pH = 3.3.

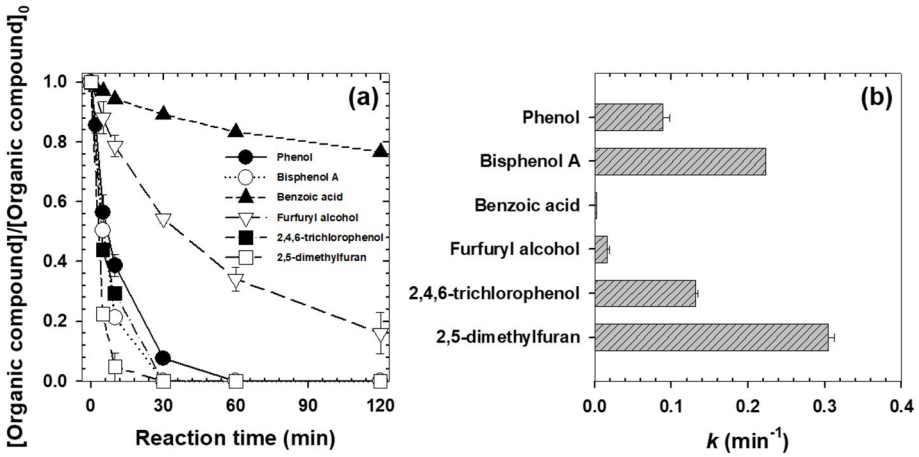

Fig. 2. (a) Degradation of various organic compounds and (b) pseudo-first-order rate constants (k) for degradation of various organic compounds by α-Fe_2O_3/PMS system: $[Phenol]_0 = [Bisphenol\ A]_0 = [Benzoic\ acid]_0 = [Furfuryl\ alcohol]_0 = [2,4,6\text{-trichlorophenol}]_0 = [2,5\text{-dimethylfuran}]_0 = 0.1$ mM; $[\alpha\text{-}Fe_2O_3]_0 = 5$ g/L; $[PMS]_0 = 1$ mM; pH = 3.3.

Table 2

Rate constants of reactive species for organic compounds.

Compound	pKa	Reactive species	Rate constant, k ($M^{-1}s^{-1}$)	Reference
Phenol	9.9	$^{\bullet}OH$	$k_{\bullet_{OH}} = 6.6 \times 10^9$	[32,34,35]
		$SO_4^{\bullet-}$	$k_{so_4^{\bullet-}} = 8.8 \times 10^9$	
		$^1O_2$	$k_{^1O_2} = 2\text{-}3 \times 10^6$	
Bisphenol A	10.3	$^{\bullet}OH$	$k_{\bullet_{OH}} = 1.55 \times 10^9$	[36]
Benzoic acid	4.2	$^{\bullet}OH$	$k_{\bullet_{OH}} = 4.3 \times 10^9$	[32,33]
		$SO_4^{\bullet-}$	$k_{so_4^{\bullet-}} = 1.2 \times 10^9$	
Furfuryl alcohol	9.6	$^{\bullet}OH$	$k_{\bullet_{OH}} = 1.5 \times 10^{10}$	[32,34]
		$^1O_2$	$k_{^1O_2} = 1.2 \times 10^8$	
2,4,6-trichlorophenol	9.6	$^{\bullet}OH$	$k_{\bullet_{OH}} = 5.48 \times 10^9$	[32,34]
		$^1O_2$	$k_{^1O_2} = 2 \times 10^6$	
2,5-dimethylfuran	-2.7	$^1O_2$	$k_{^1O_2} = 8.2 \times 10^6$	[33]

3.2. Effects of reaction parameters on phenol degradation

The experimental parameters (i.e., pH, α-Fe_2O_3 dosage, and PMS concentration) on the oxidation of phenol were investigated (Fig. 3). Complete phenol removal was achieved at pH 3.0, 7.0, and 11.0 which suggests that the α-Fe_2O_3/PMS system can be applied at a wide range of pH (Fig. 3a). The increase in α-Fe_2O_3 dosage and PMS concentration had a positive relationship on the phenol removal (Fig. 3b and Fig. 3c). The results are concerned with the activation on the surface of α-Fe_2O_3 which would be explained later.

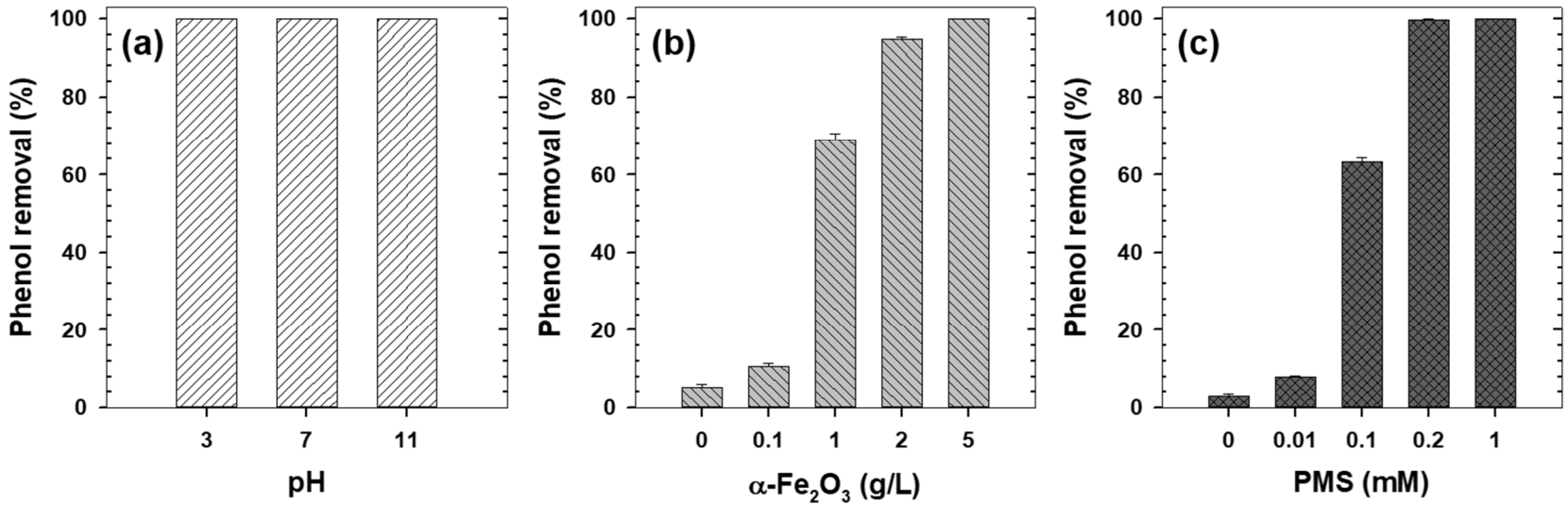

Fig. 3. (a) Phenol removal by α-Fe_2O_3/PMS system as a function of pH: $[Phenol]_0$ = 0.1 mM; $[\alpha\text{-}Fe_2O_3]_0$ = 5 g/L; $[PMS]_0$ = 1 mM; pH = 3.0 – 11.0; reaction time = 120 min. (b) Phenol removal by α-Fe_2O_3/PMS system as a function of α-Fe_2O_3 dosage: $[Phenol]_0$ = 0.1 mM; $[\alpha\text{-}Fe_2O_3]_0$ = 0 – 5 g/L; $[PMS]_0$ = 1 mM; pH = 3.3; reaction time = 120 min. (c) Phenol removal by α-Fe_2O_3/PMS system as a function of PMS concentration: $[Phenol]_0$ = 0.1 mM; $[\alpha\text{-}Fe_2O_3]_0$ = 5 g/L; $[PMS]_0$ = 0 – 1 mM; pH = 3.3; reaction time = 120 min.

The effects of experimental conditions such as dissolved oxygen in the solution and visible light illumination were investigated as well (Fig. 4). Dissolved oxygen can affect the generation of reactive oxygen species (ROS) such as superoxide radical ($O_2^{\bullet-}$) and $^1O_2$ [30]. To exclude the involvement of dissolved oxygen on the PMS activation, the solution had sparged by argon (Ar) during the experiment (Fig. 4a). Also, since α-Fe_2O_3 has exhibited photocatalytic activity [37], the experiment was conducted in a dark condition (Fig. 4b). The results suggest that dissolved oxygen and visible light illumination have a negligible effect on the PMS activation by α-Fe_2O_3.

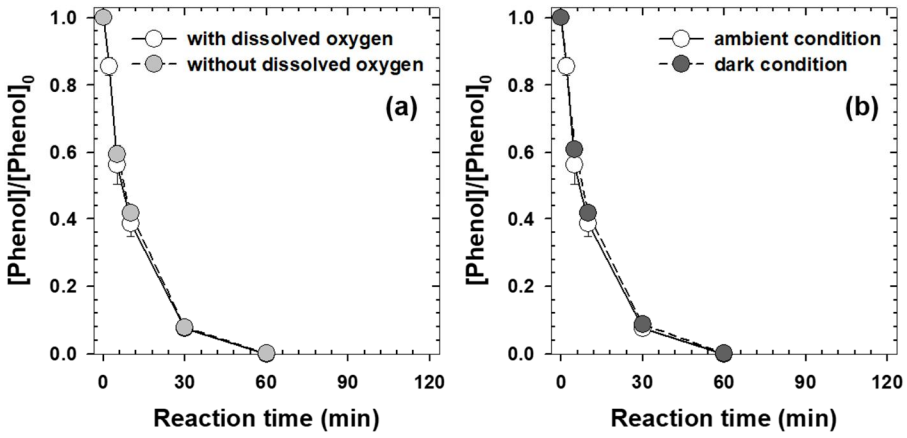

Fig. 4. (a) Degradation of phenol by α-Fe_2O_3/PMS system with and without dissolved oxygen (by sparging the solution with Ar): $[Phenol]_0$ = 0.1 mM; $[\alpha\text{-}Fe_2O_3]_0$ = 5 g/L; $[PMS]_0$ = 1 mM; pH = 3.3. (b) Degradation of phenol by α-Fe_2O_3/PMS system with and without visible light illumination: $[Phenol]_0$ = 0.1 mM; $[\alpha\text{-}Fe_2O_3]_0$ = 5 g/L; $[PMS]_0$ = 1 mM; pH = 3.3.

3.3. Mechanism of PMS activation by α-Fe_2O_3

3.3.1. Effects of scavengers

Phenol degradation in the presence of scavengers was examined. Table 3 summarizes the various scavengers and the rate constant of them. Methanol, an alcohol containing 'α-hydrogen' scavenges both $SO_4^{\bullet-}$ and $^{\bullet}OH$ ($k_{SO_4^{\bullet-}}$ = 3.2×10^6 $M^{-1}s^{-1}$ and $k_{^{\bullet}OH}$ = 9.7×10^8 $M^{-1}s^{-1}$ [32,33]). Whereas *tert*-butanol without 'α-hydrogen' is a specific $^{\bullet}OH$ scavenger ($k_{^{\bullet}OH}$ = $3.8 – 7.6 \times 10^8$ $M^{-1}s^{-1}$ [2,3]). As displayed in Fig. 5, the presence of methanol and *tert*-butanol did not inhibit the phenol degradation.

Table 3

Rate constants of scavengers for reactive species.

Scavenger	Reactive species	Rate constant, k ($M^{-1}s^{-1}$)	Reference
tert-butanol	$^{\bullet}OH$	$k_{^{\bullet}OH}$ = $3.8 – 7.6 \times 10^8$	[3]
Methanol	$^{\bullet}OH$ $SO_4^{\bullet-}$	$k_{^{\bullet}OH}$ = 9.7×10^8 $k_{SO_4^{\bullet-}}$ = 3.2×10^6	[32,33]
p-benzoquinone	$O_2^{\bullet-}$	$k_{O_2^{\bullet-}}$ = 9.8×10^8	[38]
Furfuryl alcohol	$^1O_2$	$k_{^1O_2}$ = 1.2×10^8	[34]
Azide ion (N_3^-)	$^1O_2$	$k_{^1O_2}$ = 1.0×10^9	[34]
L-histidine	$^1O_2$	$k_{^1O_2}$ = 1.5×10^8	[39]

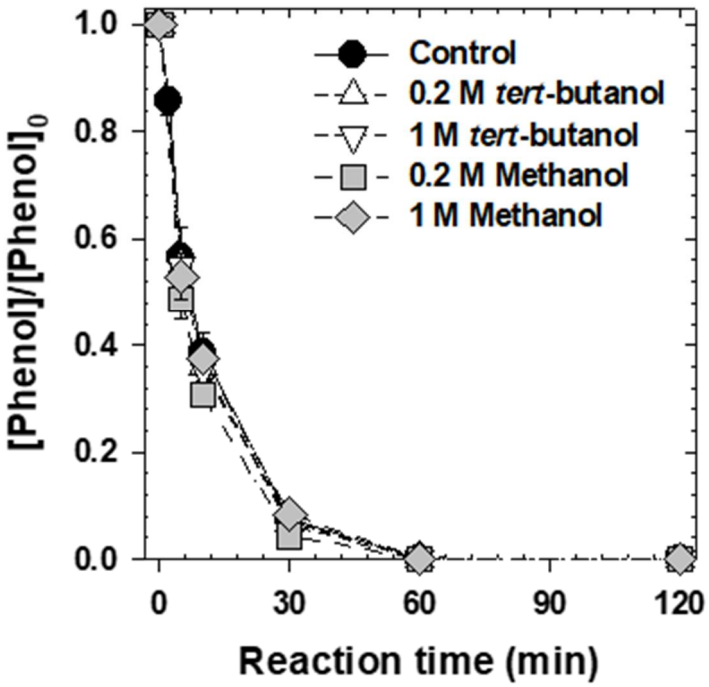

Fig. 5. Degradation of phenol by α-Fe_2O_3/PMS system with and without radical scavengers: $[Phenol]_0$ = 0.1 mM; $[\alpha\text{-}Fe_2O_3]_0$ = 5 g/L; $[PMS]_0$ = 1 mM; [*tert*-butanol]$_0$ = [Methanol]$_0$ = 0.2 – 1 M; pH = 3.3.

To evaluate the contribution of $O_2^{\bullet-}$, *p*-benzoquinone was used as an $O_2^{\bullet-}$ scavenger ($k_{O_2^{\bullet-}}$ = 9.8 × 10^8 $M^{-1}s^{-1}$ [38]) (Fig. 6a). As a result of the experiment, phenol degradation was suppressed to 48%. To ensure the participation $O_2^{\bullet-}$, probe test using XTT was examined (Fig. 6b). XTT reacts with $O_2^{\bullet-}$ to form XTT-formazan which has an absorption peak at 470 nm [40]. However, $O_2^{\bullet-}$ was not detected by XTT test. So $O_2^{\bullet-}$ is not a main reactive species in the system.

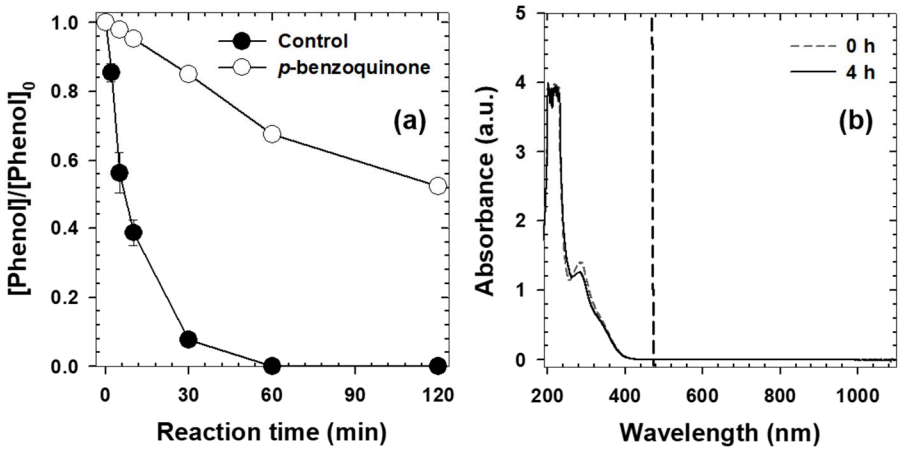

Fig. 6. (a) Degradation of phenol by α-Fe_2O_3/PMS system with and without superoxide radical scavenger: $[Phenol]_0$ = 0.1 mM; $[\alpha\text{-}Fe_2O_3]_0$ = 5 g/L; $[PMS]_0$ = 1 mM; [*p*-benzoquinone]$_0$ = 0.1 M; pH = 3.3. (b) UV-Vis absorption spectra of XTT by α-Fe_2O_3/PMS system: $[\alpha\text{-}Fe_2O_3]_0$ = 5 g/L; $[PMS]_0$ = 1 mM; $[XTT]_0$ = 1 mM; pH = 3.3; reaction time = 4 h.

The effect of $^1O_2$ scavengers (i.e. furfuryl alcohol, $k_{^1O_2}$ = 1.2 × 10^8 $M^{-1}s^{-1}$; azide ion, $k_{^1O_2}$ = 1.0 × 10^9 $M^{-1}s^{-1}$ [34]; L-histidine, $k_{^1O_2}$ = 1.5 × 10^8 $M^{-1}s^{-1}$ [39]) was examined in phenol degradation by α-Fe_2O_3/PMS system (Fig. 7a). All three $^1O_2$ scavengers inhibited phenol degradation by more than 90%. Deuterium oxide (D_2O) was used as a solvent instead of H_2O (Fig. 7b). In the D_2O solvent, the lifetime of $^1O_2$ increases tenfold, and the organic contaminant degradation by $^1O_2$ be accelerated [41]. The acceleration was not observed in D_2O suggesting that $^1O_2$ is not responsible for phenol and furfuryl alcohol degradation.

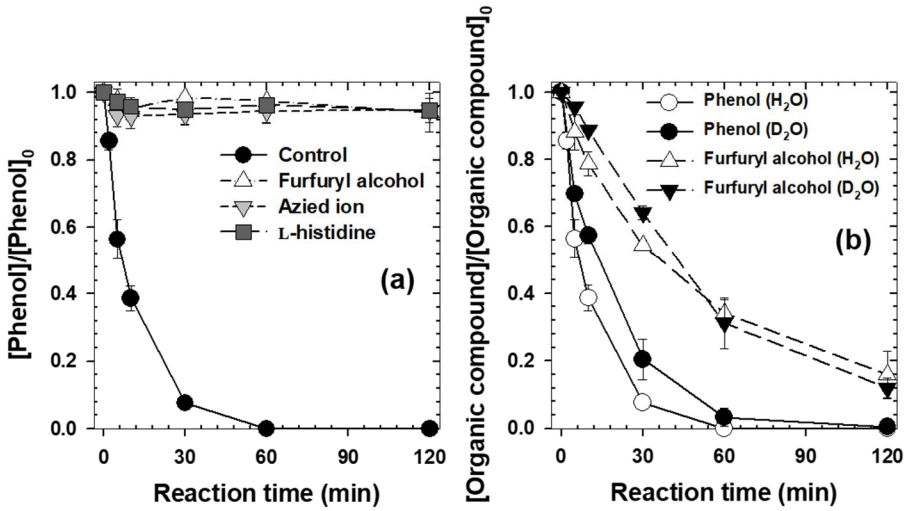

Fig. 7. (a) Degradation of phenol by α-Fe_2O_3/PMS system with and without singlet oxygen scavengers: $[Phenol]_0$ = 0.1 mM; $[\alpha\text{-}Fe_2O_3]_0$ = 5 g/L; $[PMS]_0$ = 1 mM; $[Furfuryl\ alcohol]_0$ = $[Azide\ ion]_0$ = $[L\text{-}histidine]_0$ = 0.2 M; pH = 3.3. (b) Degradation of organic compounds by α-Fe_2O_3/PMS system in the H_2O and D_2O solvent: $[Phenol]_0$ = $[Furfuryl\ alcohol]_0$ = 0.1 mM; $[\alpha\text{-}Fe_2O_3]_0$ = 5 g/L; $[PMS]_0$ = 1 mM; pH = 3.3.

3.3.2. Effects of anions

The effects of anions such as phosphate ($H_2PO_4^-$), perchlorate (ClO_4^-), nitrate (NO_3^-), and chloride (Cl^-) ions were determined (Fig. 8). $H_2PO_4^-$, which has a strong affinity and thus forms a complex with Fe(III) on the surface of the catalyst [42,43], inhibited phenol degradation about 70% with 10mM. Meanwhile, the effect of the ClO_4^-, NO_3^- and Cl^- was very minor. ClO_4^- was used to evaluate the ionic strength [43]. The little inhibition effect of ClO_4^- represents the existence of strong inner-sphere interaction between oxidant and catalyst surface. NO_3^- and Cl^- could oxidize $SO_4^{\bullet-}$ and $^{\bullet}OH$ into less active radicals (i.e., $NO_3^{\bullet}$, $NO_2^{\bullet}$, $Cl^{\bullet}$, and $Cl_2^{\bullet-}$) ((Eqs. (10)–(16)) [4,44]. The results propose that PMS activation occurs on the α-Fe_2O_3 surface, and the reactive species is neither $SO_4^{\bullet-}$ nor $^{\bullet}OH$.

$$^{\bullet}OH + NO_3^- \rightarrow OH^- + NO_3^{\bullet} \quad (10)$$

$$SO_4^{\bullet-} + NO_3^- \rightarrow SO_4^{2-} + NO_3^{\bullet} \quad (11)$$

$$NO_3^{\bullet} + H_2O + e_{aq} \rightarrow NO_2^{\bullet} + 2OH^- \quad (12)$$

$$SO_4^{\bullet-} + Cl^- \rightarrow SO_4^{2-} + Cl^{\bullet} \quad (13)$$

$$Cl^{\bullet-} + Cl^- \rightarrow Cl_2^{\bullet-} \quad (14)$$

$$Cl_2^{\bullet-} + Cl_2^{\bullet-} \rightarrow Cl_2 \quad (15)$$

$$Cl^{\bullet} + Cl^{\bullet} \rightarrow Cl_2 \quad (16)$$

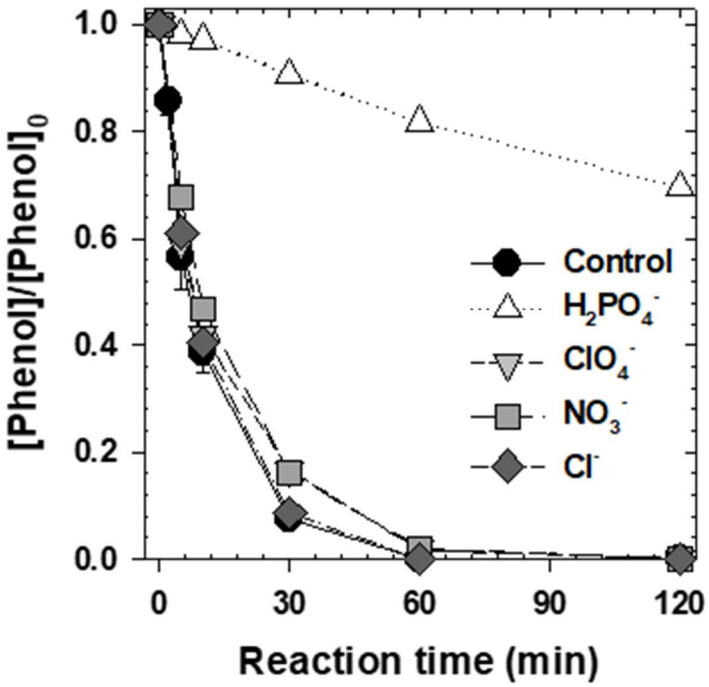

Fig. 8. Degradation of phenol by α-Fe_2O_3/PMS system with and without anions: $[Phenol]_0$ = 0.1 mM; $[\alpha\text{-}Fe_2O_3]_0$ = 5 g/L; $[PMS]_0$ = 1 mM; $[H_2PO_4^-]_0$ = $[ClO_4^-]_0$ = $[NO_3^-]_0$ = $[Cl^-]_0$ = 10 mM; pH = 3.3.

3.3.3. EPR analysis

EPR spectroscopy is a method capable of recognizing the reactive species by affirming the adduct of the spin-trapping agent. DMPO was used as a trapping agent for $SO_4^{\bullet-}$ and $^{\bullet}OH$ [45]. DMPO reacts with $SO_4^{\bullet-}$ and $^{\bullet}OH$ turn into DMPO-SO_4 and DMPO-OH adducts, respectively. While TEMPD•HCl was used to trap $^1O_2$ because Hideg et al. (2011) reported that 2,2,6,6-tetramethylpiperidine (TEMP) and 2,2,6,6-tetramethyl-4-piperidone (TEMPD) contain impurities that might affect the generation of $^1O_2$ adducts, 2,2,6,6-tetramethylpiperidine-1-oxyl (TEMPO) and 2,2,6,6-tetramethyl-4-oxo-1-piperidinyloxy (TEMPONE) [46]. The signal of 5,5-dimethyl-pyrrolidone-(2)-oxyl-(1) (DMPOX) which is corresponding to the nonradical mechanism was obtained in the α-Fe_2O_3/PMS system (Fig. 9a) [47,48]. Furthermore, no noticeable signal of $^1O_2$ was obtained in the α-Fe_2O_3/PMS system (Fig. 9b). Thusly $SO_4^{\bullet-}$, $^{\bullet}OH$, and $^1O_2$ were not the dominant reactive species for PMS activation by α-Fe_2O_3.

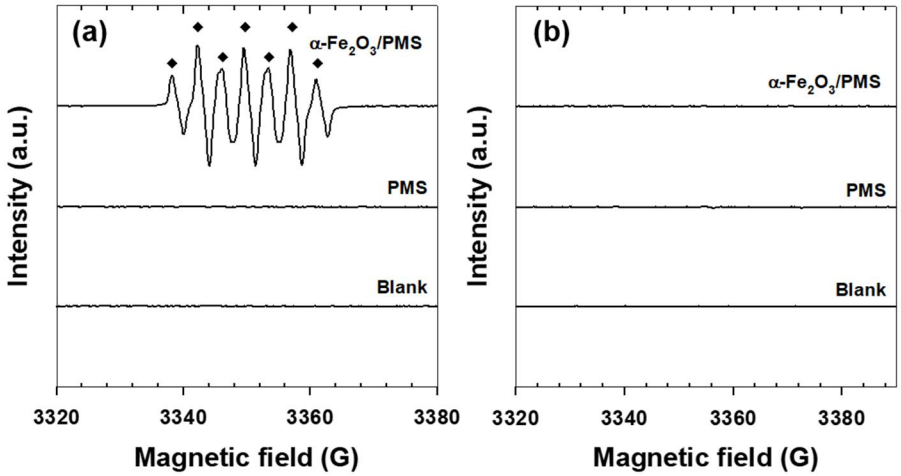

Fig. 9. (a) EPR spectra obtained by spin strapping with DMPO in the α-Fe_2O_3/PMS system: $[DMPO]_0$ = 10 mM; $[\alpha\text{-}Fe_2O_3]_0$ = 5 g/L; $[PMS]_0$ = 1 mM; pH = 3.3; reaction time = 10 min. (b) EPR spectra obtained by spin strapping with TEMPD•HCl in the α-Fe_2O_3/PMS system: $[TEMPD•HCl]_0$ = 10 mM; $[\alpha\text{-}Fe_2O_3]_0$ = 5 g/L; $[PMS]_0$ = 1 mM; pH = 3.3; reaction time = 10 min.

3.3.4. Electron mediated reactive complex

Based on the tests above, the engagement of $SO_4^{\bullet-}$, $^{\bullet}OH$, $O_2^{\bullet-}$ and $^1O_2$ which have been proposed as reactive species on the α-Fe_2O_3 related PMS activation previously are invalid. The nonradical mechanism is likely to be responsible for the α-Fe_2O_3/PMS system. Among nonradical mechanisms, electron mediated reactive complex is one of the strong candidates [49–52]. Electron mediated reactive complex is a direct two-electrons transfer from organic compound (electron donor) to persulfate (electron acceptor) on the surface of catalyst (electron mediator). Lee et al. (2015) and Kim et al (2020) conducted PDS decomposition test in the catalyst/PDS system in the presence and absence of target compound and LSV to confirm the catalyst mediated electron transfer [51,52]. The electron mediated reactive complex is a ternary system requiring all three components, hence persulfate was not decomposed in the absence of a target compound while a current increase was aroused with the addition of both target compound and PDS in LSV using catalyst coated working electrode. The PMS decomposition and LSV were examined in the presence and absence of three components of mediated electron transfer (Fig. 10). PMS decomposition was possible by α-Fe_2O_3 regardless of phenol existence (Fig. 10a). LSV showed no significant current change with the addition of PMS and phenol altogether (Fig. 10b). The result of PMS decomposition and LSV articulate that the electron mediated reactive complex does not occur.

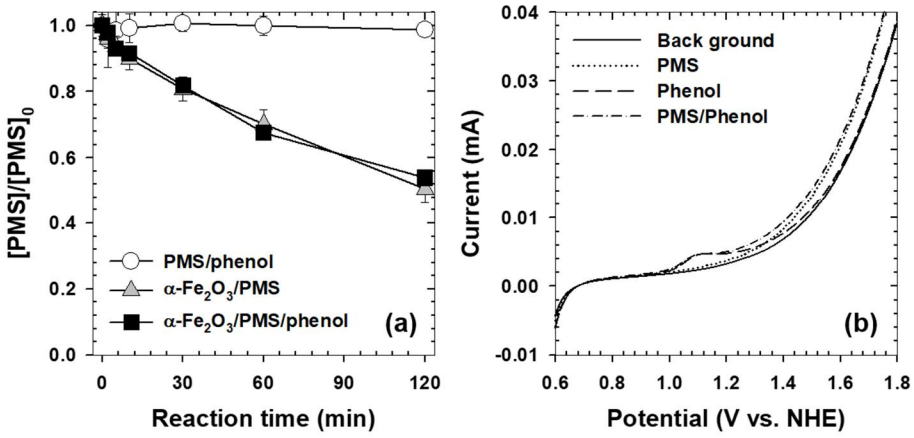

Fig. 10. (a) Decomposition of PMS in the presence of phenol or/and α-Fe_2O_3: $[Phenol]_0$ = 0.1 mM; $[\alpha\text{-}Fe_2O_3]_0$ = 5 g/L; $[PMS]_0$ = 1 mM; pH = 3.3. (b) LSV obtained by α-Fe_2O_3 coated GCE in the presence of PMS or/and phenol: working electrode = α-Fe_2O_3 coated GCE; counter electrode = Pt foil; $[Phenol]_0$ = 0.1 mM; $[PMS]_0$ = 1 mM; $[NaClO_4]_0$ = 50 mM; [dE/dt] = 20 mV/s; pH = 3.3.

3.3.5. PMS treatment of α-Fe_2O_3

To further understand the reactive species that exist on the surface of α-Fe_2O_3, the catalyst was treated with PMS. The characteristics of PMS-treated α-Fe_2O_3 were compared with pristine α-Fe_2O_3 by TEM, EDS, XRD, and zeta potential analysis (Fig. 11). No notable chemical or physical differences were observed comparing before and after the PMS treatment except for the slightly higher zeta potential of the treated one. However, PMS-treated α-Fe_2O_3 had oxidizing power to some extent without PMS (Fig. 12a). It indicates that a reactive species is existing on the surface of α-Fe_2O_3 after PMS treatment and the surface reactive species showed stability for more than 3 days (result not shown). EPR analysis expressed a signal of DMPOX in the presence of PMS-treated α-Fe_2O_3 (Fig. 12b), which supports the existence of reactive species on the surface of PMS-treated α-Fe_2O

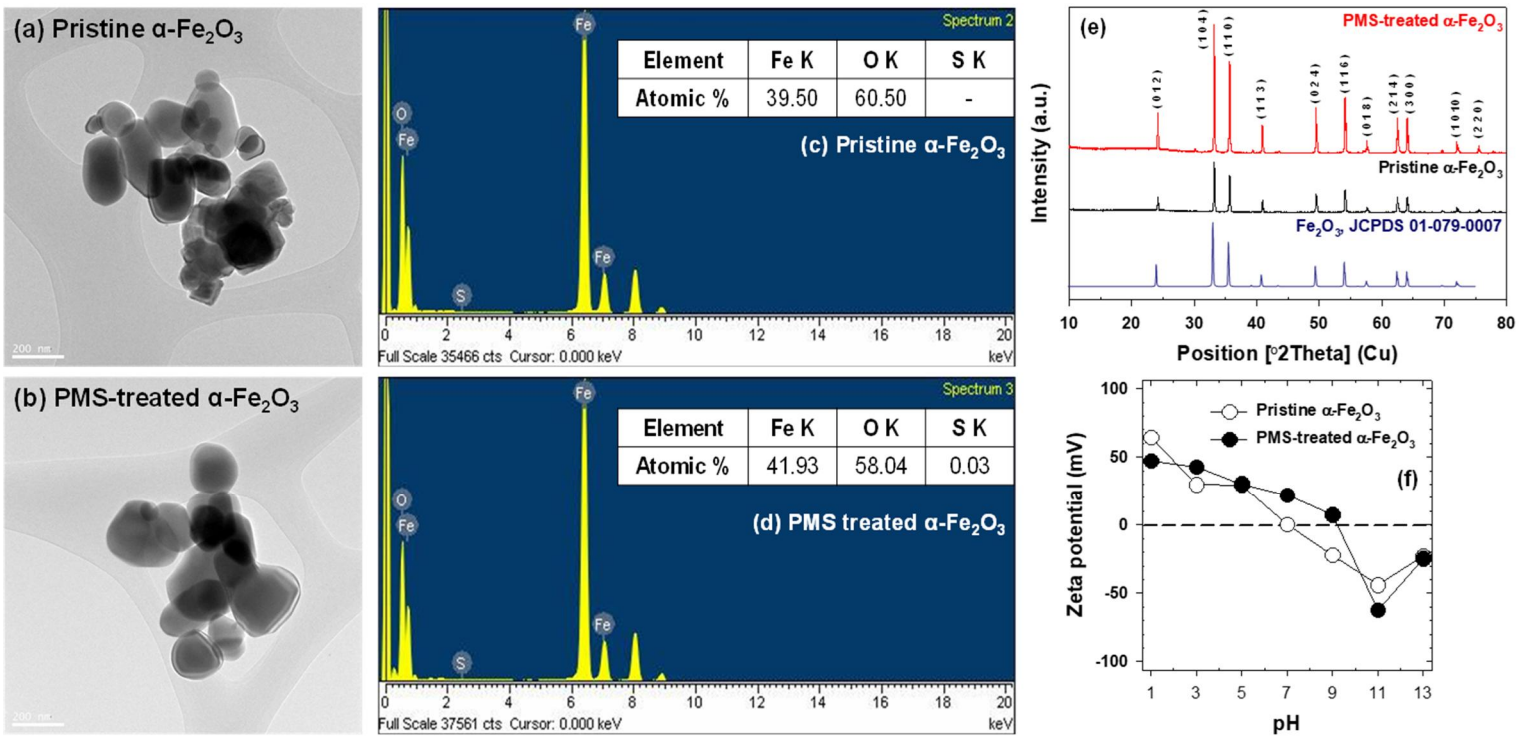

Fig. 11. (a), (b) TEM images of pristine α-Fe_2O_3 and PMS-treated α-Fe_2O_3. (c), (d) EDS analysis of pristine α-Fe_2O_3, and PMS-treated α-Fe_2O_3. (e) XRD patterns of pristine α-Fe_2O_3 and PMS-treated α-Fe_2O_3. (f) Zeta potential of pristine α-Fe_2O_3 and PMS-treated α-Fe_2O_3: $[\text{Pristine } \alpha\text{-}Fe_2O_3]_0 = [\text{PMS-treated } \alpha\text{-}Fe_2O_3]_0 = 1$ g/L; pH = 1.0 – 13.0.

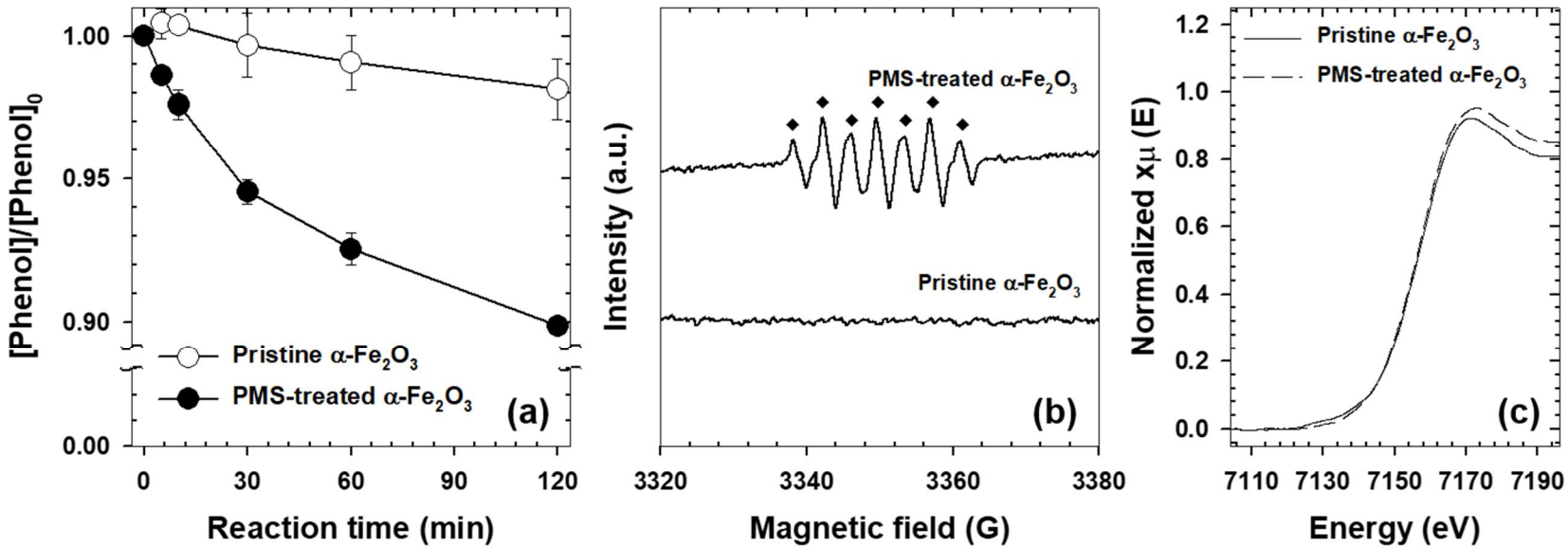

Fig. 12. (a) Degradation of phenol by pristine α-Fe_2O_3 and PMS-treated α-Fe_2O_3: $[Phenol]_0$ = 0.1 mM; $[Pristine\ \alpha\text{-}Fe_2O_3]_0$ = $[PMS\text{-}treated\ \alpha\text{-}Fe_2O_3]_0$ = 5 g/L; pH = 5.0 – 6.4. (b) EPR spectra obtained by spin strapping with DMPO in the presence of pristine α-Fe_2O_3 and PMS-treated α-Fe_2O_3: $[DMPO]_0$ = 10 mM; $[Pristine\ \alpha\text{-}Fe_2O_3]_0$ = $[PMS\text{-}treated\ \alpha\text{-}Fe_2O_3]_0$ = 50 g/L; $[PMS]_0$ = 1 mM; pH = 5.0 – 6.4; reaction time = 10 min. (c) Fe *K*-edge XANES of pristine α-Fe_2O_3 and PMS-treated α-Fe_2O_3.

The Fe *K*-edge XANES spectra of pristine α-Fe_2O_3 and PMS-treated α-Fe_2O_3 were obtained (Fig. 12c). The $1s \rightarrow 3d$ pre-edge peak and $1s \rightarrow 4p$ peak of XANES are correlated with the oxidation state [53–55]. With an increase in the oxidation state of metal oxide, $1s \rightarrow 3d$ pre-edge peak and $1s \rightarrow 4p$ peak shift to higher energy level. As shown in Fig. 12c, the $1s \rightarrow 3d$ pre-edge peak shifted by 3 eV from 7128 eV (pristine α-Fe_2O_3) to 7131 eV (PMS-treated α-Fe_2O_3) while $1s \rightarrow 4p$ peak shifted by 2 eV from 7171 eV (pristine α-Fe_2O_3) to 7173 eV (PMS-treated α-Fe_2O_3). The positive *K*-edge energy shift by 2–3 eV corresponding to the fact that the valence state is higher than Fe(III). Therefore, high-valent iron species (Fe(IV)) is speculated as a reactive species generated on the surface of α-Fe_2O_3 in the α-Fe_2O_3/PMS system.

3.3.6. High-valent iron species (Fe(IV))

Hight-valent metal species are one of the encouraging alternative persulfate activation mechanisms [49]. In previous studies, various metals such as Ag (I) and Fe(II) were reported to forms high-valent metal ions having oxidizing power [56–58]. There are a number of papers that reported the high-valent iron generation from the activation of Fe(II) ion. Wang et al. (2018, 2019) claimed the involvement of Fe(IV) in persulfate activation by Fe(II) (Eqs. (17)and(18)) [57,58]. Similarly to persulfate activation, Liang et al. (2020) suggested the production of $Fe^{IV}=O^{2+}$ from the Fe^{2+}/HOCl system through two-electron transfer (Eq. (19)) [59]. At the same time, $Fe^{IV}=O$ generation on the α-Fe_2O_3 electrode from electrochemical oxidation reaction was presented (Eqs. (20)–(23)) [60,61].

$$Fe^{2+} + HSO_5^- \rightarrow Fe^{IV}O^{2+} + SO_4^{2-} + H^+ \quad (17)$$

$$Fe^{2+} + S_2O_8^- \rightarrow Fe^{IV}O^{2+} + 2SO_4^{2-} + 2H^+ \quad (18)$$

$$Fe^{2+} + HOCl \rightarrow Fe^{IV}O^{2+} + HCl \quad (19)$$

$$\equiv Fe^{III} + H_2O \rightarrow \equiv Fe^{III}–OH + H^+ \quad (20)$$

$$\equiv Fe^{III}–OH \rightarrow \equiv Fe^{IV}O^{2+} + H^+ + e^- \quad (21)$$

$$\equiv Fe^{III} + H_2O_2 + H_2O \rightarrow \equiv Fe^{IV}O^{2+} + O_2 + 4H^+ + 3e^- \quad (22)$$

$$\equiv Fe^{III}–OH + H_2O_2 \rightarrow \equiv Fe^{IV}O^{2+} + O_2 + 3H^+ + 3e^- \quad (23)$$

The formation of Fe(IV) was determined by electrochemical analysis using α-Fe_2O_3 modified CPE (Fig. 13a). A reversible couple with redox potential at 1.21 V *vs.* NHE and a small reversible couple with redox potential at 0.71 V *vs.* NHE appeared. From the bare CPE experiment with Fe^{+3} ion, it is conjecturable that the reversible couple with $E°$ = 0.71 V *vs.* NHE is Fe(II)/Fe(III) redox couple (Fig. 13b). Thus, the reactive species from the α-Fe_2O_3/PMS system has an $E°$ value of 1.21 V *vs.* NHE. Previous studies have reported the redox potential of Fe^{IV}=O(-chelate)/Fe(III)(-chelate) complex at near the 1.2 V *vs.* NHE [61–65].

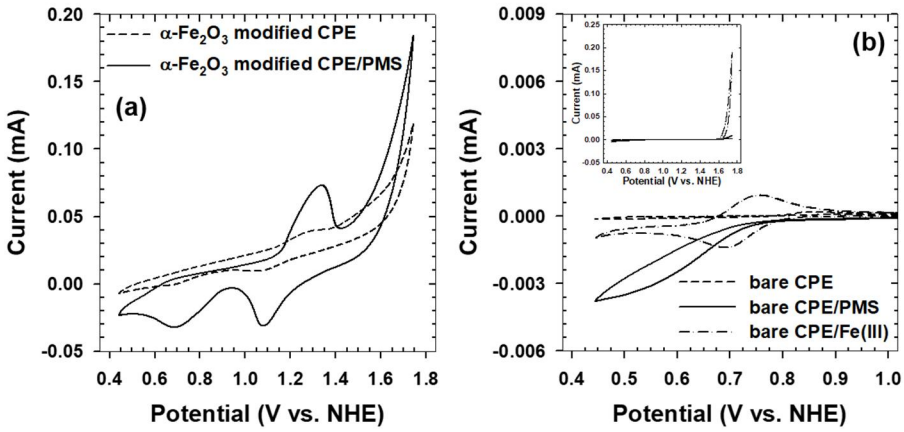

Fig. 13. (a) CV by α-Fe_2O_3 modified CPE with and without PMS: working electrode = α-Fe_2O_3 modified CPE; counter electrode = Pt mesh; $[PMS]_0$ = 25 mM; $[NaClO_4]_0$ = 500 mM; [dE/dt] = 2 mV/s; pH = 3.3. (b) CV by bare CPE with and without PMS and Fe(III): working electrode = bare CPE; counter electrode = Pt mesh; $[PMS]_0$ = 25 mM; $[Fe(III)]_0$ = 5 mM; $[NaClO_4]_0$ = 500 mM; [dE/dt] = 2 mV/s; pH = 3.3.

A strong reducing agent, hydroxylamine (HA) could convert surface Fe(III) to Fe(II) and enhance the Fenton-like reaction [29]. When HA was added to the α-Fe_2O_3/PMS system, the phenol degradation was decelerated and even the 200 mM of radical scavengers could inhibit the reaction (Fig. 14). Thus, the Fe(II) would not engage in the Fe(IV) generation.

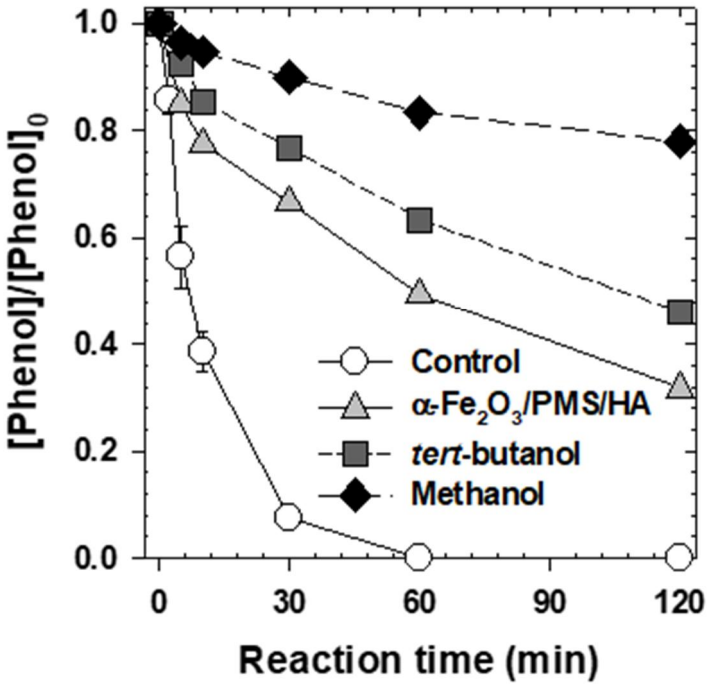

Fig. 14. Degradation of phenol by α-Fe_2O_3/PMS system with and without hydroxylamine and radical scavengers: $[Phenol]_0$ = 0.1 mM; $[\alpha\text{-}Fe_2O_3]_0$ = 5 g/L; $[PMS]_0$ = 1 mM; $[Hydroxylamine]_0$ = 1 mM; [*tert*-butanol]$_0$ = $[Methanol]_0$ = 200 mM; pH = 3.3.

Based on the above results, surface Fe(III) on the α-Fe_2O_3 is the main source of high-valent oxoiron(IV) during the PMS activation. The possible pathway for Fe^{IV}=O generation from surface Fe(III) via one-electron transfer was proposed in Eq. (24). PMS is decomposed on the process of Fe^{IV}=O generation without generating radical species or $^1O_2$ (Fig. 10a) [66]. The generated Fe^{IV}=O acts as a main oxidizing species for organic compounds degradation.

$$2{\equiv}Fe^{III}{-}OH + HSO_5^- \rightarrow 2{\equiv}Fe^{IV}O^{2+} + SO_4^{2-} + H_2O + H^+ \qquad (24)$$

The generated Fe^{IV}=O has a redox potential of 1.21 V *vs.* NHE. Though the oxidizing potential is lower than radical species ($E°(^{\bullet}SO_4^{\bullet-}/SO_4^{2-})$ = 2.43 V *vs.* NHE and $E°(^{\bullet}OH/H_2O)$ = 2.81 V *vs.* NHE [6,67]), it has higher selectivity than nonselective radical species [59,68]. Thus, the α-Fe_2O_3/PMS system is a suitable method for the degradation of various organic contaminants due to prominent activity and substrate-specific tendency.

4. Conclusions

This study demonstrated that the α-Fe_2O_3/PMS system can adequately oxidize organic compounds in an aqueous system. In general, α-Fe_2O_3 was more effectual than other iron-based catalysts. The pH, dissolved oxygen, and light illumination did not affect the activation mechanism of the α-Fe_2O_3/PMS system significantly. Diverse experiments using scavengers, XTT, D_2O, anions, EPR spectroscopy, and LSV indicated that the system is generating neither radical species (i.e., $SO_4^{\bullet-}$, $^{\bullet}OH$, and $O_2^{\bullet-}$), $^1O_2$ nor electron mediated reactive complex. XANES and CV declared that the Fe^{IV}=O generated on the surface of α-Fe_2O_3 is the dominant reactive species for the degradation of phenol among the nonradical mechanisms. The α-Fe_2O_3/PMS system is weakly affected by pH change and has a higher selectivity toward some organic compounds. Thus, the α-Fe_2O_3/PMS system is a promising way to wastewater treatment and soil remediation.

References

[1] F. Ghanbari, M. Moradi, Application of peroxymonosulfate and its activation methods for degradation of environmental organic pollutants. Chem. Eng. J. 310 (2017) 41–62.

[2] G.P. Anipsitakis, D.D. Dionysiou, Degradation of organic contaminants in water with sulfate radicals generated by the conjunction of peroxymonosulfate with cobalt, Environ. Sci. Technol. 37 (2003) 4790–4797.

[3] G.P. Anipsitakis, D.D. Dionysiou, Radical generation by the interaction of transition metals with common oxidants, Environ. Sci. Technol. 38 (2004) 3705–3712.

[4] G.P. Anipsitakis, D.D. Dionysiou, M.A. Gonzalez, Cobalt-mediated activation of peroxymonosulfate and sulfate radical attack on phenolic compounds. Implications of chloride ions, Environ. Sci. Technol. 40 (2006) 1000-1007.

[5] M. Spiro, The standard potential of the peroxosulphate/sulphate couple, Electrochim. Acta 24 (1979) 313–314.

[6] R.E. Huie, C.L. Clifton, P. Neta, Electron transfer reaction rates and equilibria of the carbonate and sulfate radical anions, Radiat. Phys. Chem. 38 (1991) 477–481.

[7] A.R. Gallopo, J.O. Edwards, Kinetics and mechanism of the oxidation of pyridine by caro's acid catalyzed by ketones, J. Org. Chem. 46 (1981) 1684–1688.

[8] G. Manivannan, P. Maruthamuthu, Kinetics and mechanism of

oxidation of aliphatic and aromatic ketones by peroxomonosulphate, J. Chem. Soc. Perkin Trans. 2 4 (1986) 565–568.

[9] C. Lee, H.H. Kim, N.B. Park, Chemistry of persulfates for the oxidation of organic contaminants in water, Membr. Water Treat. 9 (2018) 405–419.

[10] S. Yang, P. Wang, X. Yang, L. Shan, W. Zhang, X. Shao, R. Niu, Degradation efficiencies of azo dye Acid Orange 7 by the interaction of heat, UV and anions with common oxidants: persulfate, peroxymonosulfate and hydrogen peroxide, J. Hazard. Mater. 179 (2010) 552–558.

[11] C. Qi, X. Liu, J. Ma, C. Lin, X. Li, H. Zhang, Activation of peroxymonosulfate by base: implications for the degradation of organic pollutants, Chemosphere 151 (2016) 280–288.

[12] Y.H. Guan, J. Ma, X.C. Li, J.Y. Fang, L.W. Chen, Influence of pH on the formation of sulfate and hydroxyl radicals in the UV/peroxymonosulfate system, Environ. Sci. Technol. 45 (2011) 9308-9314.

[13] C. Cai, H. Zhang, X. Zhong, L. Hou, Ultrasound enhanced heterogeneous activation of peroxymonosulfate by a bimetallic Fe–Co/SBA-15 catalyst for the degradation of Orange II in water, J. Hazard. Mater. 283 (2015) 70–79.

[14] F. Ji, C. Li, X. Wei, J. Yu, Efficient performance of porous Fe_2O_3 in heterogeneous activation of peroxymonosulfate for decolorization of Rhodamine B, Chem. Eng. J. 231 (2013) 434–440.

[15] R.D.C. Soltani, M. Mashayekhi, S. Jorfi, A. Khataee, M.J.

Ghanadzadeh, M. Sillanpää, Implementation of martite nanoparticles prepared through planetary ball milling as a heterogeneous activator of oxone for degradation of tetracycline antibiotic: ultrasound and peroxy-enhancement, Chemosphere 210 (2018) 699–708.

[16] A. Rastogi, S.R. Al-Abed, D.D. Dionysiou, Effect of inorganic, synthetic and naturally occurring chelating agents on Fe(II) mediated advanced oxidation of chlorophenols, Water Res. 43 (2009) 684–694.

[17] M. Zhang, F. He, D. Zhao, X. Hao, Degradation of soil-sorbed trichloroethylene by stabilized zero valent iron nanoparticles: effects of sorption, surfactants, and natural organic matter, Water Res. 45 (2011) 2401–2414.

[18] A. Bhattacharyya, A.N. Campbell, M.M. Tfaily, Y. Lin, R.K. Kukkadapu, W.L. Silver, P.S. Nico, J. Pett-Ridge, Redox fluctuations control the coupled cycling of iron and carbon in tropical forest soils, Environ. Sci. Technol. 52 (2018) 14129–14139.

[19] N. Sabri, K. Hanna, V. Yargeau, Chemical oxidation of ibuprofen in the presence of iron species at near neutral pH, Sci. Total Environ. 427–428 (2012) 382–389.

[20] D. Ding, C. Liu, Y. Ji, Q. Yang, L. Chen, C. Jiang, T. Cai, Mechanism insight of degradation of norfloxacin by magnetite nanoparticles activated persulfate: identification of radicals and degradation pathway, Chem. Eng. J. 308 (2017) 330–339.

[21] F. Sepyani, R.D.C. Soltani, S. Jorfi, H. Godini, M. Safari, Implementation of continuously electro-generated Fe_3O_4 nanoparticles for activation of persulfate to decompose amoxicillin antibiotic in

aquatic media: UV_{254} and ultrasound intensification, J. Environ. Manage. 224 (2018) 315–326.

[22] R.L. Rudnick, S. Gao. Composition of the continental crust, in: R.L. Rudnick, H.D. Holland, K.K. Turekian, Treatise on geochemistry 3: The crust, Elsvier, Amsterdam, 2003, pp. 1–64.

[23] M. Yu, A.L. Teel, R.J. Watts, Activation of peroxymonosulfate by subsurface minerals, J. Contam. Hydrol. 191 (2016) 33–43.

[24] N. Jaafarzadeh, F. Ghanbari, M. Ahmadi, Catalytic degradation of 2,4-dichlorophenoxyacetic acid (2,4-D) by nano-Fe_2O_3 activated peroxymonosulfate: influential factors and mechanism determination, Chemosphere 169 (2017) 568–576.

[25] W.D. Oh, S.K. Lua, Z. Dong, T.T. Lim, High surface area DPA-hematite for efficient detoxification of bisphenol A via peroxymonosulfate activation, J. Mater. Chem. A 2 (2014) 15836–15845.

[26] J. Virkutyte, R.S. Varma, Eco-friendly magnetic iron oxide-pillared montmorillonite for advanced catalytic degradation of dichlorophenol, ACS Sustain. Chem. Eng. 2 (2014) 1545–1550.

[27] H. Zheng, J. Bao, Y. Huang, L. Xiang, Faheem, B. Ren, J. Du, M.N. Nadagouda, D.D. Dionysiou, Efficient degradation of atrazine with porous sulfurized Fe_2O_3 as catalyst for peroxymonosulfate activation, Appl. Catal. B: Environ. 259 (2019) 118056.

[28] Y. Feng, C. Liao, H. Li, C. Liu, K. Shih, Cu_2O-promoted degradation of sulfamethoxazole by α-Fe_2O_3-catalyzed peroxymonosulfate under circumneutral conditions: synergistic effect, Cu/Fe ratios, and

mechanisms, Environ. Technol. 39 (2018) 1–11.

[29] W. Sang, Z. Li, M. Huang, X. Wu, D. Li, L. Mei, J. Cui, Enhanced transition metal oxide based peroxymonosulfate activation by hydroxylamine for the degradation of sulfamethoxazole, Chem. Eng. J. 383 (2020) 123057.

[30] S. Guo, H. Wang, W. Yang, H. Fida, L. You, K. Zhou, Scalable synthesis of Ca-doped α-Fe2O3 with abundant oxygen vacancies for enhanced degradation of organic pollutants through peroxymonosulfate activation, Appl. Catal. B: Environ. 262 (2020) 118250.

[31] C. Liang, C.F. Huang, N. Mohanty, R.M. Kurakalva, A rapid spectrophotometric determination of persulfate anion in ISCO, Chemosphere, 73 (2008) 1540–1543.

[32] G. V. Buxton, C.L. Greenstock, W.P. Helman, A.B. Ross, Critical review of rate constants for reactions of hydrated electrons, hydrogen atoms and hydroxyl radicals ($^{\bullet}OH/^{\bullet}O^{-}$ in aqueous solution, J. Phys. Chem. Ref. Data. 17 (1988) 513–886.

[33] P. Neta, V. Madhavan, H. Zemel, R.W. Fessenden, Rate constants and mechanism of reaction of $SO_4^{\bullet-}$ with aromatic compounds, J. Am. Chem. Soc. 99 (1977) 163–164.

[34] F.E. Scully, J. Hoigné, Rate constants for reactions of singlet oxygen with phenols and other compounds in water, Chemosphere 16 (1987) 681–694.

[35] J. Ziajka, W. Pasiuk-Bronikowska, Rate constants for atmospheric trace organics scavenging $SO_4^{\bullet-}$ in the Fe-catalysed autoxidation of S (IV), Atmos. Environ. 39 (2005) 1431–1438.

[36] N. Nakatani, N. Hashimoto, H. Sakugawa, An evaluation of hydroxyl radical formation in river water and the potential for photodegradation of bisphenol A, in: R.J. Hill, The Geochemical society special publications series 9: Geochemical investigations in Earth and space science: a tribute to Isaac R. Kaplan, Elsvier, Amsterdam, 2004, pp. 233–242.

[37] C. Kormann, D.W. Bahnemann, M.R. Hoffmann, Environmental photochemistry: is iron oxide (hematite) an active photocatalyst? A comparative study: α-Fe_2O_3, ZnO, TiO_2, J. Photochem. Photobiol. A: Chemistry, 48 (1989) 161–169.

[38] P.S. Rao, E. Hayon, Experimental determination of the redox potential of the superoxide radical $^{\bullet}O_2^-$, Biochem. Biophys. Res. Commun. 51 (1973) 468–473.

[39] F. Wilkinson, J.G. Brummer, Rate constants for the decay and reactions of the lowest electronically excited singlet state of molecular oxygen in solution, J. Phys. Chem. Ref. Data 10 (1981) 809–999.

[40] L. Brunet, D.Y. Lyon, E.M. Hotze, P.J.J. Alvarez, M.R. Wiesner, Comparative photoactivity and antibacterial properties of C_{60} fullerenes and titanium dioxide nanoparticles, Environ. Sci. Technol. 43 (2009) 4355–4360.

[41] P.B. Merkel, R Nilsson, D.R. Kearns, Deuterium effects on singlet oxygen lifetimes in solutions. A new test of singlet oxygen reactions, J. Am. Chem. Soc. 94 (1972) 1030–1031.

[42] Y. Ren, L. Lin, J. Ma, J. Yang, J. Feng, Z. Fan, Sulfate radicals induced from peroxymonosulfate by magnetic ferrospinel MFe_2O_4 (M = Co, Cu,

Mn, and Zn) as heterogeneous catalysts in the water, Appl. Catal. B: Environ. 165 (2015) 572–578.

[43] Y. Xu, J. Ai, H. Zhang, The mechanism of degradation of bisphenol A using the magnetically separable $CuFe_2O_4$/peroxymonosulfate heterogeneous oxidation process, J. Hazard. Mater. 309 (2016) 87–96.

[44] J. Li, M. Xu, G. Yao, B. Lai, Enhancement of the degradation of atrazine through $CoFe_2O_4$ activated peroxymonosulfate (PMS) process: kinetic, degradation intermediates, and toxicity evaluation, Chem. Eng. J. 348 (2018) 1012–1024.

[45] M.J. Davies, B.C. Gilbert, J.K. Stell, A.C. Whitwood, Nucleophilic substitution reactions of spin adducts. Implications for the correct identification of reaction intermediates by EPR/spin trapping. J. Chem. Soc. Perkin Trans. 2 3 (1992) 333–335.

[46] É. Hideg, Z. Deák, M. Hakala-Yatkin, M. Karonen, A.W. Rutherford, E. Tyystjärvi, I. Vass, A. Krieger-Liszkay, Pure forms of the singlet oxygen sensors TEMP and TEMPD do not inhibit Photosystem II, Biochim. Biophys. Acta 1807 (2011) 1658–1661.

[47] R.A. Floyd, L.M. Soong, Spin trapping in biological systems. Oxidation of the spin trap 5,5-dimethyl-1-pyrroline-1-oxide by a hydroperoxide-hematin system, Biochem. Biophys. Res. Commun. 74 (1977) 79–84.

[48] G.M. Rosen, E.J. Rauckman, Spin trapping of the primary radical involved in the activation of the carcinogen *N*-hydroxy-2-acetylaminofluorene by cumene hydroperoxide-hematin, Mol. Pharmacol. 17 (1980) 233–238.

[49] J. Lee, U. von Gunten, J.H. Kim, Persulfate-based advanced oxidation: critical assessment of opportunities and roadblocks, Environ. Sci. Technol. 54 (2020) 3064–3081.

[50] T. Zhang, Y. Chen, Y. Wang, J. Le Roux, Y. Yang, J.P. Croué, Efficient peroxydisulfate activation process not relying on sulfate radical generation for water pollutant degradation, Environ. Sci. Technol. 48 (2014) 5868–5875.

[51] H. Lee, H.J. Lee, J. Jeong, J. Lee, N.B. Park, C. Lee, Activation of persulfates by carbon nanotubes: oxidation of organic compounds by nonradical mechanism, Chem. Eng. J. 266 (2015) 28–33.

[52] H.H. Kim, D. Lee, J. Choi, H. Lee, J. Seo, T. Kim, K.M. Lee, A.L.T. Pham, C. Lee, Nickel–nickel oxide nanocomposite as a magnetically separable persulfate activator for the nonradical oxidation of organic contaminants, J. Hazard. Mater. 388 (2020) 121767.

[53] J. Wong, F.W. Lytle, R.P. Messmer, D.H. Maylotte, *K*-edge absorption spectra of selected vanadium compounds, Phys. Rev. B, 30 (1984) 5596.

[54] A. Corrias, G. Ennas, G. Mountjoy, G. Paschina, An X-ray absorption spectroscopy study of the Fe K edge in nanosized maghemite and in Fe_2O_3–SiO_2 nanocomposites, Phys. Chem. Chem. Phys. 2 (2000) 1045–1050.

[55] A.J. Berry, H.S.C. O'Neill, K.D. Jayasuriya, S.J. Campbell, G.J. Foran, XANES calibrations for the oxidation state of iron in a silicate glass, Am. Miner. 88 (2003) 967–977.

[56] F. Minisci, A. Citterio, C. Giordano, Electron-transfer processes: peroxydisulfate, a useful and versatile reagent in organic chemistry, Acc.

Chem. Res. 16 (1983) 27–32.

[57] Z. Wang, J. Jiang, S. Pang, Y. Zhou, C. Guan, Y. Gao, J. Li, Y. Yang, W. Qiu, C. Jiang, Is sulfate radical really generated from peroxydisulfate activated by iron(II) for environmental decontamination?, Environ. Sci. Technol. 52 (2018) 11276–11284.

[58] Z. Wang, W. Qiu, S. yan Pang, Y. Zhou, Y. Gao, C. Guan, J. Jiang, Further understanding the involvement of Fe(IV) in peroxydisulfate and peroxymonosulfate activation by Fe(II) for oxidative water treatment, Chem. Eng. J. 371 (2019) 842–847.

[59] S. Liang, L. Zhu, J. Hua, W. Duan, P.T. Yang, S.L. Wang, C. Wei, C. Liu, C. Feng, Fe^{2+}/HClO reaction produces $Fe^{IV}O^{2+}$: an enhanced advanced oxidation process, Environ. Sci. Technol. 54 (2020) 6406–6414.

[60] O. Zandi, T.W. Hamann, Determination of photoelectrochemical water oxidation intermediates on haematite electrode surfaces using operando infrared spectroscopy, Nat. Chem. 8 (2016) 778–783.

[61] K. Kamiya, A. Kuwabara, T. Harada, S. Nakanishi, Electrochemical formation of Fe(IV)= O derived from H_2O_2 on a hematite electrode as an active catalytic site for selective hydrocarbon oxidation reactions, Chem. Phys. Chem. 20 (2019) 648–650.

[62] V.K. Sharma, Oxidation of inorganic contaminants by ferrates (VI, V, and IV)–kinetics and mechanisms: a review, J. Environ. Manage. 92 (2011) 1051–1073.

[63] D. L. Popescu, M. Vrabel, A. Brausam, P. Madsen, G. Lente, I. Fabian, A.D. Ryabov, R. van Eldik, T.J. Collins, Thermodynamic,

electrochemical, high-pressure kinetic, and mechanistic studies of the formation of oxo Fe^{IV}– TAML species in water, Inorg. Chem. 49 (2010) 11439–11448.

[64] W. P. To, T.W.S. Chow, C.W. Tse, X. Guan, J.S. Huang, C.M. Che, Water oxidation catalysed by iron complex of *N,N′*-dimethyl-2,11-diaza[3,3](2,6) pyridinophane. Spectroscopy of iron–oxo intermediates and density functional theory calculations. Chem. Sci. 6 (2015) 5891–5903.

[65] W.H. Koppenol, J.F. Liebman, The oxidizing nature of the hydroxyl radical. A comparison with the ferryl ion (FeO^{2+}), J. Phys. Chem. 88 (1984) 99–101.

[66] H.H. Kim, H. Lee, D. Lee, Y.J. Ko, H. Woo, J. Lee, C. Lee, A.L.T. Pham, Activation of hydrogen peroxide by a titanium oxide-supported iron catalyst: evidence for surface Fe(IV) and its selectivity, Environ. Sci. Technol. 54 (2020) 15424–15432.

[67] A.J. Bard, R. Parsons, J. Jordan, Standard Potentials in Aqueous Solution, Marcel Dekker, New York, 1985.

[68] H. Li, C. Shan, W. Li, B. Pan, Peroxymonosulfate activation by iron(III)-tetraamidomacrocyclic ligand for degradation of organic pollutants via high-valent iron-oxo complex, Water Res. 147 (2018) 233–241.

요약(국문초록)

헤마타이트(α-Fe_2O_3)는 일과황산염(PMS)을 활성화시켜 다양한 수중 유기오염물질을 산화 분해하는 것으로 알려졌다. 헤마타이트에 의해 활성화된 일과황산염은 페놀류를 효과적으로 분해한다. 페놀 분해에 대한 pH, 촉매 주입량, 산화제 농도의 영향이 평가되었다. 본 실험 결과는 설페이트 라디칼과 하이드록실 라디칼 같은 라디칼 종에 반대되는 증거를 제시한다. 라디칼 스캐빈저, XTT, 음이온, 전자스핀 공명 분광기를 이용한 실험은 이전에 제시된 라디칼 메커니즘이 아님을 제시한다. 일중항산소 스캐빈저 실험은 페놀 분해를 억제할 수 있지만 전자스핀 공명 분광기 분석과 중수 실험에 의해 일중항산소의 가능성을 부정할 수 있다. 또한, 헤마타이트에 의한 PMS 분해와 전기화학적 분석은 전자전달 매게 복합체로의 역할을 하지 않음을 뒷받침한다. 본 실험 결과는 헤마타이트/일과황산염 시스템에 의한 유기 오염물질의 활성 반응 종으로 고원자가 철을 제시한다. 헤마타이트 표면에서 생성된 4가철이 유기오염물질을 산화 분해하는 역할을 한다.

주요어 : 일과황산염, 헤마타이트, 산화, 유기 오염물질, 비라디칼 메커니즘, 고원자가 철

학 번 : 2019-27656

감사의 글

대학원 생활 가운데 지도해 주시고 응원해주신 모든 분들께 감사드립니다.